Hilbert Huang and Wavelet Processing of Time Domain Signals from Ultrasoinc Guided Waves Magnetostrictive Sensors Arrays

Sami Barmada, Antonino Musolino, Marco Raugi, Mauro Tucci, and Florin Turcu

Abstract— In this paper we compare the effectiveness of the time, wavelet and Hilbert Huang domain analysis of waveforms from a Non Destructive Test (NDT) equipment. The analysis of the signals from NDT systems is one of the most important activities since it allows to locate the actual defects. Very often the echoes traveling back to the sensors are superimposed with the signal from the transducer. We analyze the waveforms obtained by couples of sensors in order to extract the echoes and to recognize the points were they originate. A preliminary numerical analysis has been used to study the main features of the elastic waves propagations in inhomogeneous materials

Keywords— Non Destructive Test, Hilbert Huang transform, Magnetostrictive transducers and sensors, Ultrasonic waves, Wavelet transform.

I. INTRODUCTION

ULTRASOUNDS based techniques have been introduced for long range NDT in different engineering fields [1], [2]. In particular, in the case of plants with systems of pipes, ultrasonic torsional waves, guided by the walls of the pipes themselves, have been used to inspect portions of pipes up to 20 meters long. The presence of a defect in the structure produces an echo detected by properly positioned sensors. Although the position of the defects can be evaluated with sufficient precision, very little can be said about the extension and the shape that are, if necessary, investigated with other techniques thus reducing the time needed to complete the investigation.

We propose the same approach for the NDT analysis of concrete or masonry walls; the first step would consist of the inspection of a relatively large portion of the structure with the aim of detecting and locate possible defects. The extension and the shape of the defect can be subsequently investigated by the use of the signal processing techniques on a narrow zone.

The feasibility of a long distance inspection technique for concrete structure based on the propagation of the elastic ultrasonic waves has been investigated by the authors in previous papers [3], [4]. We will now focus on the analysis of the signals detected by the sensors that is crucial to the practical feasibility of the proposed approach.

The presence of a defect produces an echo traveling back to the transducer. We can also consider the defect as a secondary source that activates when the wavefront from the transducer impacts the defect itself. The presence of superior modes across the thickness of the wall (when its thickness is comparable with the wavelength of the excitation) and the multiple reflections between the boundary surfaces makes it difficult to identify the echo in the waveform by sensor. However, if the sensors are placed at two points close to each other, it is possible to recognize the presence of a backward traveling wave by performing a proper comparison of the two waveforms. The knowledge of the arrival instants of the backward waves on an array of couples of sensors makes it possible to estimate the position of the defect. A correct estimate of the arrival instant is then crucial for a good performance of the triangulation algorithm that is usually used.

The accuracy of the results produced by time domain analysis of the couple of waveforms from the sensors may be improved by performing further analysis in the wavelet and Hilbert Huang domains.

II. THEORETICAL ANALYSIS

In order to asses the validity of the proposed long range inspection technique several numerical analysis of the propagation of elastic waves have been performed both on concrete and brick masonry walls. We simulated the action of the transducer by imposing a tangential force on a small portion of the surface of the walls. Magnetostrictive transducers driven by known currents have been used in the experimental campaign. The waveform shown in fig. 1 has been used in all the simulations. The force is zero for instants after 0.12 ms.

We considered a concrete wall 4 meters high (y direction), 1.5 meters long (x direction) with a thickness of 15 centimeters. The transducer is located in the centre of the upper surface. It is 2 centimeters high and 10 centimeters long and is able to transmit an x-directed force to the underlying portion of the surface. Table I shows the physical constant assumed for the concrete.
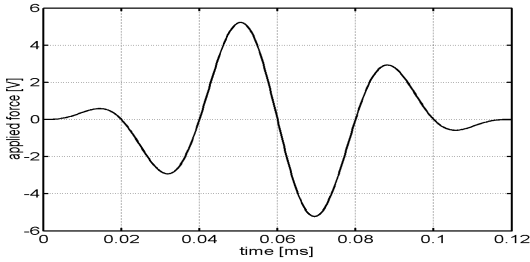
Fig. 1. Time waveform of the transducer driving current; the transmitted force is proportional.

Elasticity modulus	E=2.2E+10	N/m^2
Poisson ratio	ν =0.15	
Mass density	ρ=2.4E+3	kg/m^3
Damping parameters	α_M=5.0E-04	s^{-1}
	α_K= 1.0 E-08	s
Lamè parameters	μ_L=9.56 E+09	N/m^2
	λ_L= 4.099E+09	

Table 1. Concrete data.

Because of the symmetries only the upper half of the structure has been simulated. We started by performing the simulation of the propagation of an elastic wave on the wall without defects [5], [6]. Successively we examined two configurations characterized by the presence of defects of different shapes and in different positions. Firstly we considered a defect consisting of a void long 10 cm and high 3 cm that passes through the wall on its entire thickness. Two positions have been chosen; the first one at the coordinates x=0, y=1 (the middle of the shown portion of the geometry), the second at at x=-0.4 and y=1.0.
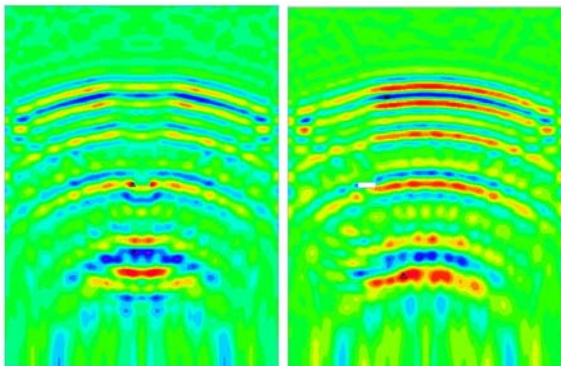
Fig. 2. X axis component of the displacement at various times instant for the wall with the void. The first image refers to the wall with central void at 0.78 ms, the second to the void in the left hand portion of the wall at 0.78 ms.

Figures 2 shows the color maps of the computed x-displacement at properly selected instants. The effects of the presence of the defects are evident. In particular it is possible to recognize the presence of waves that travel from the defect

backward to the transducer. TAll these images provide important information on the propagation of the elastic waves in the structure under test. In particular it is possible to locate the regions that are "lighted" by the transducer; this helps in the choice of the positioning of the sensors. Obviously these images are not available when performing a realistic measurement as they would require a huge number of sensors for their construction while the number of sensors seldom exceeds ten. As the thickness of the wall is greater (about twice) than the wavelength at 30 kHz, higher order modes appear in the propagation of the elastic waves. The response of the wall does not consist of a single pulse shaped similarly to the excitation force traveling from the transducer but lasts for a mach longer time than that shown in fig. 1. The wavefront of the echo reflected by the defect is then superimposed with the tail of the wave from the transducer and this may hide the echo itself. What it is clear at a first glance form fig. 2 it is very difficult to reconstruct by the information taken by a reasonable number of sensors.

III. EXPERIMENTAL SETUP

All the experimental data have been obtained by measurements campaign performed by using the diagnostic system MsS 2020® shown in fig. 3 with its transducer sensor [7].

Fig. 3. The MsS 2020® system and its transducer sensor

This apparatus, based on magnetostrictive transducers and sensors, is able to produce the propagation of transversal guided waves in the frequency range 4-128 kHz. A nickel strip is glued on the surface of the wall and is properly magnetized by using a rare earts permanent magnet. A coil driven by the system MsS 2020® is placed over the strip. Because of the strong magnetostrictive properties of the nickel, a current flowing on the coil is able to produce a deformation on the nickel strip that is transmitted to the wall. The operation of the can be reversed: a displacement of the magnetized nickel strip is able to induce an electromotive force at the terminals of the coil.

IV. MULTIPATH MODEL FOR WAVE PROPAGATION

Let us consider two points A and B as shown fig 4a. The position of the transducer is known as well as the thickness of the wall. We also assume the knowledge of the transverse velocity of the elastic waves. Propagation is not purely transversal, as a consequence the formula

$v = \sqrt{E/(2\rho(\upsilon+1))}$ could not be used as it represents only a rough estimate. It is however possible to obtain a better estimate of the velocity by a contextual measurement. In the case of the presence of a forward traveling wave only it is possible to relate the waveforms at points A and B; by properly delaying the curve at point A it is expected to become very similar to that at point B.
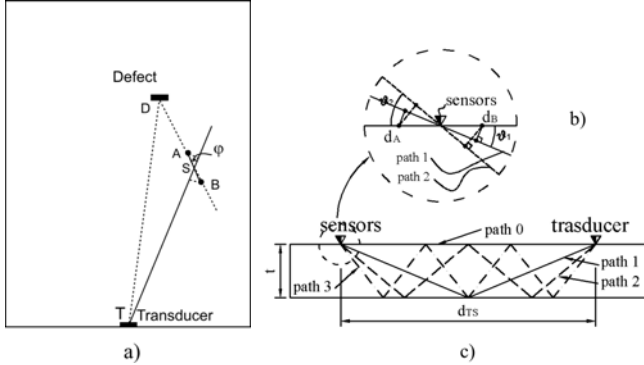
Fig. 4. a) Experimental setup for the concrete wall; b) schematic position of transducer, defect and sensors couple, c) multipath model.

The presence of a backward traveling wave due to the echo from the defect prevents this occurrence and, as a consequence, may be used as a proof of the presence of the defect.

The delay times may be evaluated by using a simple model based on the different lengths of the multiple paths that exist between the transducer and the sensors.

Let us consider the projection of the distance between the two points on the direction connecting the center of the transducer with S, the midpoint of A and B.

$$\Delta s = \overline{AB}\cos\varphi \qquad (1)$$

If we recall the shape of the wavefront in the Figures 2, Δs can be considered the distance between A and B as seen by the transducer. Let us now consider the cross section of the wall corresponding to the segment TS as shown in fig. 4b that shows the direct path and a few other paths between the transducer and the mid point of A and B. Let d_A and d_B be the distances form the transducer to the projections of A and B

on TS respectively. The length of TS is $d_{TS} = 0.5 \cdot (d_A + d_B)$. The delay of the direct path is $\Delta t_0 = (d_A - d_B)/v$, ($v$ is the transversal velocity), that of the path #k is

$$\Delta t_k = ((d_A - d_B)\cos\theta_k)/v; \quad \theta_k = tg^{-1}((2kt)/d_{TS}) \quad (2)$$

as shown in fig. 4b.

These different (decreasing) delays are assigned to different portions of the waveform by the following rule. Δt_0 is assigned to the portion of curve that starts at time $t_0 = l_0/v$ where l_0 is the length of the direct path (see fig. 4b) and lasts $\Delta T = 0.12\,ms$ sec (the time interval where the excitation is not zero, as reported in fig. 2). Δt_k is assigned to the portion of curve that starts at time

$$t_k = \frac{l_k}{v} = \frac{2k}{v}\sqrt{t^2 + \left(\frac{d_A + d_B}{4k}\right)^2} \qquad (3)$$

and lasts $\Delta T = 0.12\,ms$ (l_k is the length of the path #k).

The correspondence built by this rule is a piecewise constant function. Once a proper smoothing is performed, the curve of the displacements at point A is accordingly shifted to obtain a curve that is almost coincident with that at point B.

An example of the waveforms related to the concrete wall with the void in the upper position and detected by a couple of sensors at 70 and 73 cm from the transducer (aligned with the transducer and the defect) are shown in figs. 5 and 6. The curves in fig. 6 are coincident until the instant $\overline{t} = 1.3 \cdot 10^{-3}$ sec. This means that at this instant the reflected wave from the defect has reached the sensors couple after traveling from the transducer to the defect and back to the sensors: $d_{tot} = d_{TD} + d_{DS} \simeq 2.82 \simeq \overline{t} \cdot v = 1.3 \cdot 10^{-3} \cdot 2180$. The recognition of the arrival instant of the echo from the defect by comparison of the time waveforms above shown may lead to inaccurate results. The accuracy may be increased by performing the product of the waveforms as in fig. 6
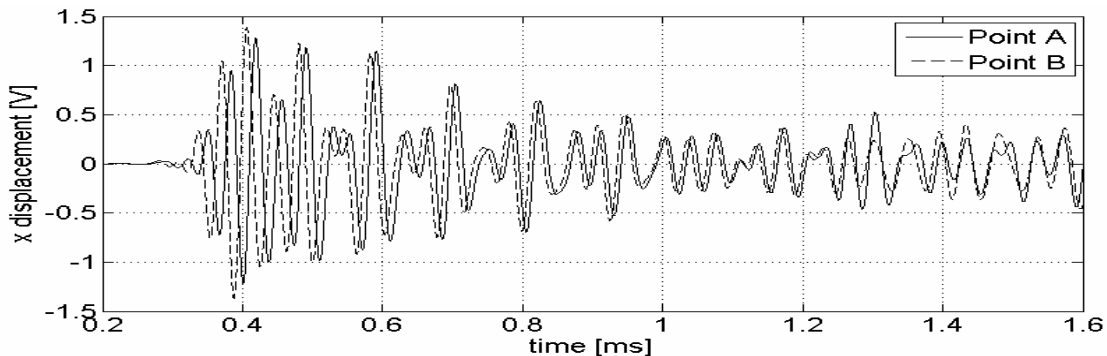
Fig. 5. *X*-displacements at points A and B (vertical axis unit is volt)
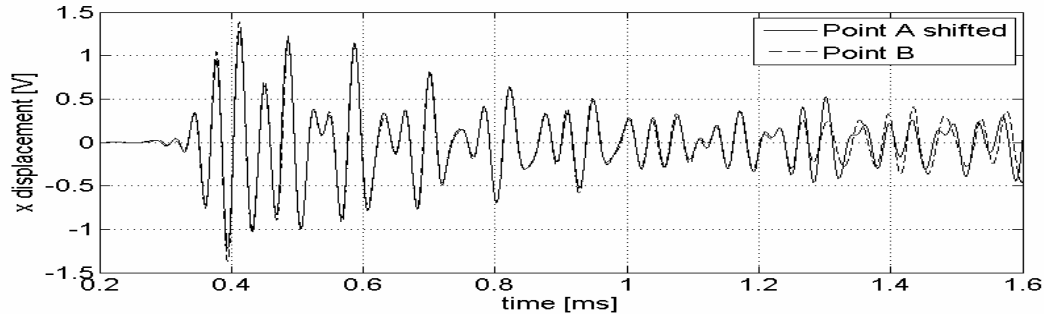
Fig. 6. Comparison of the *x*-displacements at point B and point A shifted

When the two curves are both of the same sign the product assumes positive values, while negative values are related to the existence of a phase difference between the factors. The improvement in the accuracy by using the product is not fully satisfactory. The analysis of the signals by the Hilbert-Huang transform and by the wavelet transform will be investigated too.

V. DATA ANALYSIS

An experimental campaign has been performed on a concrete wall shown in fig. 7.

The numerical results shown in fig. 2a describe with good approximation the interaction between the couple transducer defect D2 T2; 2b is related to T3 D2. S1 denotes the couple of sensors whose measured waveforms are shown in figs. 5 and 6.

Figure 8 shows the displacement at the sensors of the couple in S2 when T2 is active. An inspection of the curves shown in fig. 8 reveals a phase difference occurring for the first time around $t_0 = 0.8\ ms$. This occurrence may me evidenced by considering the product of the curves as shown in fig. 9. We see that the product assumes for the first time negative values near t_0.

$$T_1 \equiv (-0.75, 0.0)$$
$$T_2 \equiv (0.75, 0.0)$$
$$T_3 \equiv (0.40, 0.0)$$
$$D_1 \equiv (-0.75, 1.80)$$
$$D_2 \equiv (0.75, -1.0)$$
$$S_1 \equiv \begin{pmatrix} -0.75, 0.70 \\ -0.75, 0.73 \end{pmatrix}$$
$$S_2 \equiv \begin{pmatrix} 0.45, -0.515 \\ 0.45, -0.555 \end{pmatrix}$$
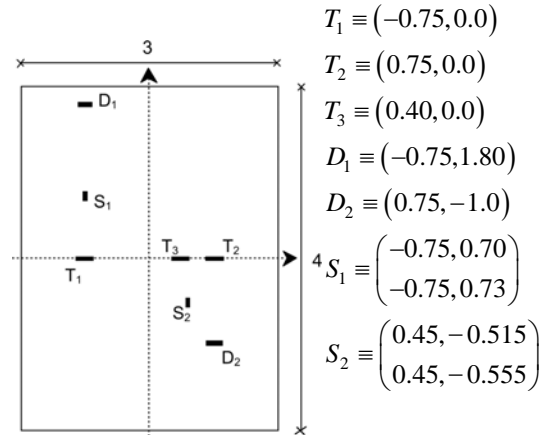
Fig. 7. Dimensions of the concrete specimen and position of the transducers, defects and sensors used in the experimental measurements. The centre of the wall was assumed as the origin of the coordinates.

A better localization of the instant where the phase difference starts can be performed by comparing the sensors waveform in the wavelet and in the Hilbert-Huang domains [8], [9].
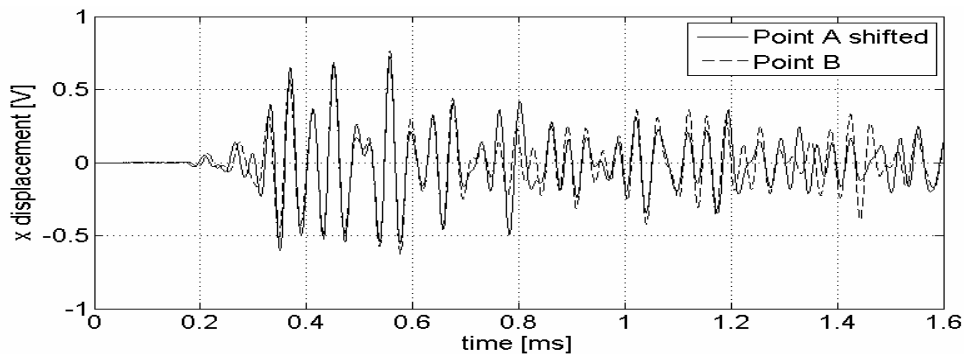
Fig. 8. X-displacements at sensors of the couple in S2 (vertical axis unit is volt)
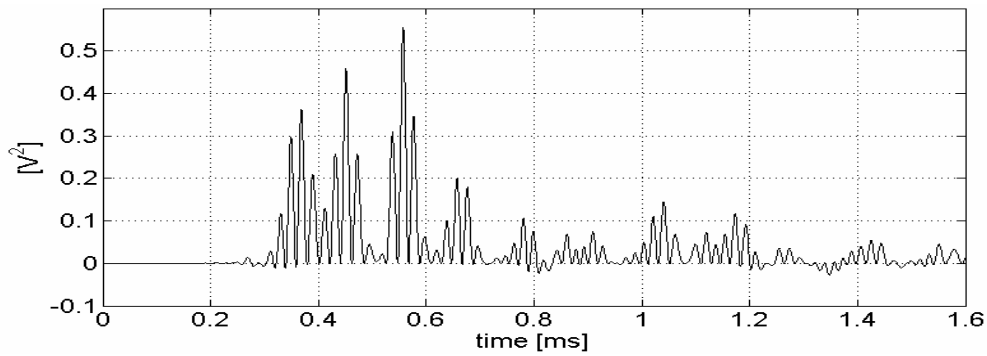
Fig. 9. Product of the displacements measured by the sensors.

Let us begin with the wavelet transform. We used Daubechies wavelet on the interval with NV=6 vanishing moments and compared the details the curves at different levels. For a better understanding of the figures we report only the portions of the curves in the interval *0.5-1.0 ms.* The occurrence of the phase difference can be acknowledged at all the detail level with increasing resolution. In particular fig. 10 c) clearly shows the phase difference between the two signals in the interval $[0.73 \cdot 10^{-3}, 0.8 \cdot 10^{-3}]$.
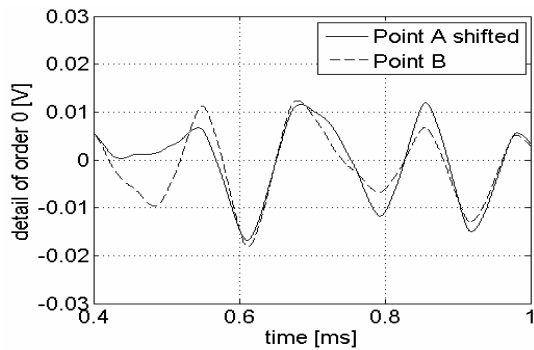
(a)
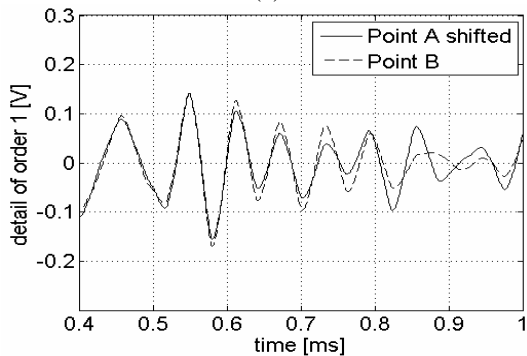
(b)
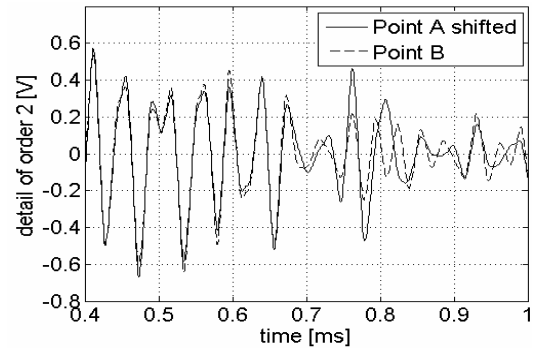
(c)
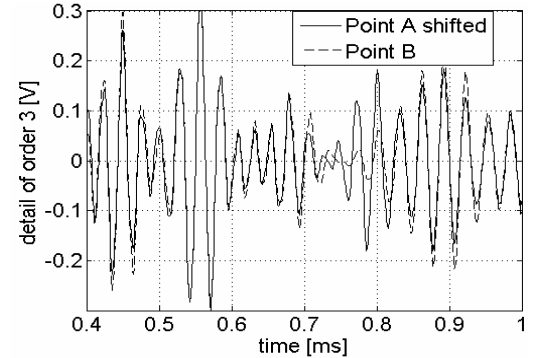
(d)

Fig. 10. Comparison of the blurred version (a) and of the details of the signals (b-d)

The comparison in the Hilbert-Huang domain is carried on by comparing the EMF for the two signals. As the EMF functions of the form $a(t)\sin(p(t))$ it is possible to define instantaneous phase and frequency and this allows an accurate location of the instants of phase variation of one signal with respect to the other.

Figure 11 shows the comparison of the waveforms of the first two EMFs of the signals that are those characterized by the highest frequency content. The other EMFs contain low frequency information and do not permit a sufficient focusing on the time domain. Figure 12 shows the instantaneous frequency of the EMFs of fig. 111. The phase variation of one signal with respect to the other is clearly evidenced by the peaks.

(a)

b)
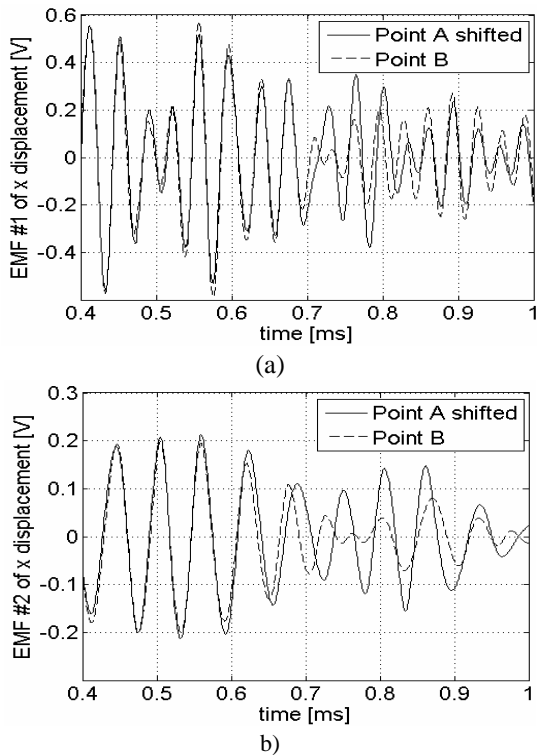
Fig. 11. Comparison of the first two EMFs.

(a)

(b)
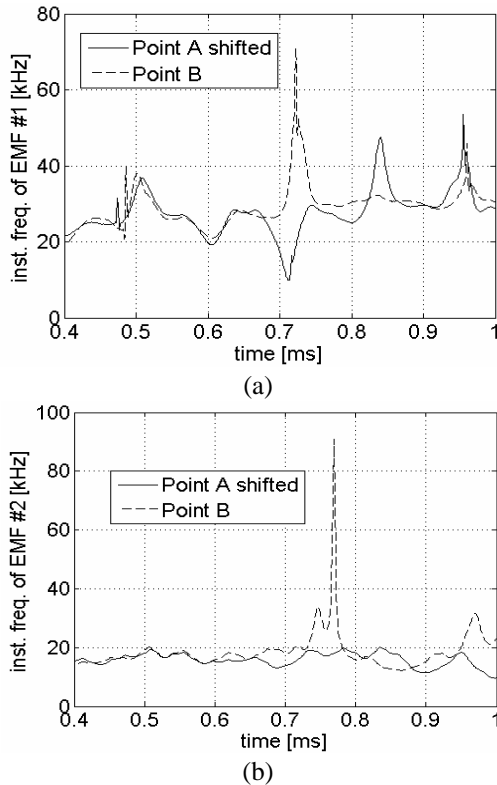
Fig. 12. Comparison of the instantaneous frequency of the first two EMFs

The rough estimate of $t_0 \simeq 0.78\,ms$ obtained by the analysis of the waveforms in the time domain has been refined by the use of the wavelet transform that allows a more precise evaluation by considering together the figs. 15 c) and d) that suggests the new estimate $t_0 \simeq 0.74\,ms$. The analysis of the instantaneous frequency content of the EMFs obtained by the Hilbert-Huang transform provide a further estimate $t_0 \simeq 0.72\,ms$ that is the time instant where in both figures 17 a) and b) a strong phase variation of one signal with respect to the other appears for the first time.

If, as shown in fig. 12, we consider the total distance $D_{tot} = \overline{T_2 D_2} + \overline{D_2 S_2} \simeq 1.55\,m$ and assume $v \simeq 2218\,m/s$ as the velocity of the elastic wave (contextually measured) we find by using the t_0 above estimated $D_{meas} = v \cdot t_0 = 1.60\,m$ that is very close to D_{tot}.

This confirms the validity of the proposed approach based on the Hilbert-Huang transform.

VI. CONLCUSION

A comparison between time, wavelet and Hilbert-Huang domain analysis of data from ultrasonic nondestructive test for concrete wall has been presented. The analysis performed by using the Hilbert-Huang transform has demonstrated as the more reliable one. Nevertheless a comparative analysis of the results obtained by all the three examined techniques can help in obtaining even more precise and reliable results..

REFERENCES

[1] Shuller, M. P.: Nondestructive testing and damage assessment of masonry structures, Prog. Struct. Engng Mater. 5, 239–251 (2003)
[2] Cawley, P., Alleyne, D.: Practical Long Range Guided Wave Inspection - Managing Complexity", in Review of Quantitative Nondestructive Evaluation, 22, 22-37, (2003)
[3] Musolino A., Raugi M., Tucci M., Turcu F.: "Feasibility of Defect Detection in Concrete Structures via Ultrasonic Investigation" Progress in Electromagnetic Research Symposium, August 27-30, 2007 Prague, Czech Republic, pp.371-375
[4] Musolino A., Raugi M., Tucci M., Turcu F.: "Voids Detection in Brick Masonry Structures by Using Ultrasonic Testing." IEEE Ultrasonic Symposium pp.: 1377 – 1380, New York, 28-31 Oct. 2007
[5] Kaltenbacher, M.: "Numerical Simulation of Mechatronic Sensors and Actuators." Spriger, Berlin (2004).
[6] Graff K. F.: "Wave Motion in Elastic Solids", Oxford University Press (1975)
[7] Operating and technical instructions for magnetostrictive sensor(MSS) instrumentation system, model MsSR2020, MsSR2020D, prepared by Sensor Systems and NDE Technology Department, Applied Physics Division, South West Research Institute, San Antonio, Texas - December 2004.
[8] Huang, N. E., Z. Shen, S. R. Long, M. C. Wu, H. H. Shih, Q. Zheng, N.-C. Yen, C. C. Tung, H. H. Liu,: The empirical mode decomposition and the Hilbert spectrum for nonlinear and non-stationary time series analysis. Proc. R. Soc. London, Ser. A, 454, 903–995 (1998).
[9] Daubechies. I.: Ten Lectures on Wavelets. Philadelphia, PA, SIAM (1992).

Sami Barmada received the Master and Ph.D. degrees in electrical engineering from the University of Pisa, Pisa, Italy, in 1995 and 2001, respectively.

From 1995 to 1997, he was with ABB Teknologi, Oslo, Norway, where he was involved with distribution network analysis and optimization. He is currently an Associate Professor with the Department of Electrical System and Automation, University of Pisa, where he is involved with numerical computation of electromagnetic fields, particularly on the modeling of multiconductor transmission lines and to the application of wavelet expansion to computational electromagnetics.

Prof. Barmada was General Chairman of the ACES 2007 conference in Verona, Italy and the technical chairman of the Progress In Electromagnetic Research Symposium (PIERS), Pisa, Italy, 2004 and has served as chairman and session organizer of international conferences. He currently is a member of the BoD of the ACES Society.

He was the recipient of the 2003 J F Alcock Memorial Prize, presented by The Institution of Mechanical Engineering, Railway Division, for the best paper in technical innovation.

Antonino Musolino received the Master degree in Electronic Engineering and the Ph. D degree in Electrical Engineering from the University of Pisa in 1990 and 1995 respectively.

He is currently an Associate Professor of electrical engineering with the Department of Electrical Systems and Automation, University of Pisa. His main research activities are the numerical methods for the analysis of electromagnetic fields in linear and nonlinear media, the design of special electrical machines and the application of the WE to computational electromagnetics.

Marco Raugi received the degree in Electronic Engineering from the University of Pisa in 1985 and the Ph. D. in Electrical Engineering from the Department of Electrical Systems and Automation in 1990 where he is currently a full professor of Electrical Engineering.

His research activity is in the numerical methods for the analysis of electromagnetic fields in linear and nonlinear media. Main applications have been devoted to Non Destructive Testing, Electromagnetic compatibility in transmission lines He is author of around 100 papers on international journals and conferences.

He has been the general chairman of the ISPLC (International Symposium on PowerLine Communications) 26-28 March 2007 in Pisa, and the general chairman of the international conference PIERS (Progress In Electromagnetic Research Symposium) 28-31 March 2004 in Pisa. In the mainframe of international conferences (ACES, COMPUMAG, CEFC, ISPLC, PIERS) he served as chairman, session organizer, author of invited lectures, instructor of courses and tutorials, member or chairman of editorial boards. He has been recipient of the IEEE-Industry Application Society 2002 Melcher Prize Paper Award.

Mauro Tucci received the degree in Automation Engineering from the University of Pisa in 2004 and at present he is a student in the international PhD course "Applied Electromagnetism in electrical and biomedical engineering, electronics, smart sensors, nano-technologies" at the Department of Electrical Systems and Automation of the University of Pisa. His research activity is in machine learning, data analysis, and system identification, with applications in electromagnetism, Non Destructive Testing, and power-lines communications.

Florin O. Turcu has a BSc degree in Physics and an MSc in Biophysics and Medical Physics granted by the University of Bucharest, Romania in 2003 and 2005 respectively. During 2005 he was the beneficiary of a 12 month research grant from the World Federation of Scientists (WFS), in the frame of the National Scholarship Programme. In 2007 Florin O. Turcu became a member of the Italian Society of Physics. In March 2008 he received his PhD degree in applied electromagnetism, at the University of Pisa, Italy. He is currently a postdoctoral researcher at the Department of Electrical Systems and Automation, University of Pisa. His research interests include design and development of innovative sensors and advanced techniques for long-range NDE by means of Ultrasonic Guided Waves.